VARIAN associates
611 HANSEN WAY · PALO ALTO, CALIF.

RADC-TDR-63-194

HIGH POWER R-F WINDOW STUDY PROGRAM

QUARTERLY TECHNICAL NOTE NO. 3

1 January Through 31 March 1963

VARIAN ASSOCIATES
Palo Alto, California

Contract No. AF 30(602)-2844
Project No. 5573
Task No. 557303

Prepared by: Floyd Johnson
Approved by: L. T. Zitelli

Prepared For

ROME AIR DEVELOPMENT CENTER
AIR FORCE SYSTEMS COMMAND
RESEARCH AND TECHNOLOGY DIVISION
UNITED STATES AIR FORCE
GRIFFISS AIR FORCE BASE
NEW YORK

VARIAN REPORT NO. 304-3Q

April 1963

Copy No. 20

ABSTRACT

A study was made into the possibilities of waveguide window synthesis by computer solution of a multiple complex matrice equation. In general, waveguide windows can be described in terms of shunt susceptances, lengths of waveguide (dielectric or air loaded), and dielectric interfaces. The T_{21} and T_{22} transmission parameters which form a part of the solution to such an equation can be used to minimize the reflection coefficient of a window.

A 100 per cent bubble-free fused quartz window was fabricated and tested in the ring resonator. This window became visibly red hot at 190 kilowatt cw, which is about twice the power level at which failure occurred in several previously tested windows made of a poorer grade of quartz. Another difference in this test was that the quartz itself did not deform.

One single disc, zero degree cut, synthetic sapphire window assembly was completed. It has not yet been high power tested but provision has been made, by the design of a special reuseable, bakeable vacuum flange, to use it as one half of a windowtron. The windowtron is to be composed of the sapphire window, any other bakeable window assembly and a 5 liter VacIon® pump. The first window scheduled for testing in the windowtron was completed this quarter. It is composed of two AL300 discs and can be cooled with either a gaseous or liquid dielectric.

The broadbanding of half-wavelength block windows was examined and a complete example of the process for a beryllium oxide window is demonstrated. Techniques for mode shifting and impedance matching are discussed. One sample of a BeO block window was tested, without failure, to 222 kilowatts cw in the ring resonator.

Several half-wavelength block windows fabricated using AL300, AL399 and AL995 ceramics were tested to failure in the ring resonator. The failure in all cases is a vertical crack across the center of the face of the block and perpindicular to the broadwall. The power level at which these failures occurred was approximately 100 kilowatts.

Title of Report RADC-TDR-63-194

PUBLICATION REVIEW

This report has been reviewed and is approved.

Approved: James H. Baldwin
for Lt Col USAF
ARTHUR J. FROHLICH
Chief, Techniques Laboratory
Directorate of Aerospace Surveillance & Control

Approved: James H. Baldwin
for Lt Col USAF
WILLIAM T. POPE
Acting Director
Director of Aerospace
Surveillance & Control

TABLE OF CONTENTS

Section		Page No.
I.	OBJECTIVES OF PROGRAM	1
	1-1. INTRODUCTION	1
	1-2. OBJECTIVES	1
	A. Primary	1
	B. Third Quarter Objectives	1
II.	TECHNICAL PROGRESS OF PROGRAM	3
	2-1. GENERAL DISCUSSION	3
	A. Conferences	3
	B. Window Synthesis by Computer Solution	3
	2-2. WINDOW CONSTRUCTION AND HIGH POWER TESTING	9
	A. Single Thin Disc Fused Quartz Windows	9
	B. Single Thin Disc Sapphire Windows	9
	C. Double Thin Disc Windows	13
	D. Half-Wavelength Beryllium Oxide Windows	13
	E. Half-Wavelength Aluminum Oxide Windows	22
	F. Windowtron Resonant Ring Testing	28
III.	PROGRAM FOR NEXT QUARTER	30
IV.	REFERENCES	31
	APPENDIX	33

LIST OF ILLUSTRATIONS

Figure		Page No.
1	WINDOW CONFIGURATIONS	4
2	FOUR TERMINAL NETWORK REPRESENTATION OF A WAVEGUIDE WINDOW	6
3	SYMONS-TYPE THIN DISC WINDOW	6
4	CROSS SECTION OF TEST JIGS USED TO MEASURE TRANSITION PARAMETERS z_1, z_2, and z_3	8
5	POWER DISSIPATION IN QUARTZ THIN DISC WINDOW	10
6	SINGLE DISC SAPPHIRE WINDOW ASSEMBLY	11
7	SINGLE DISC SAPPHIRE WINDOW CHARACTERISTICS	12
8	DOUBLE DISC AL300 WINDOW ASSEMBLY	14
9	DOUBLE DISC AL300 WINDOW CHARACTERISTICS	15
10	POWER DISSIPATION IN NATIONAL BERYLLIA HIGH DENSITY BeO BLOCK WINDOW	17
11	ADMITTANCE PLOTS OF X-BAND BeO BLOCK WINDOW	19
12	ADMITTANCE PLOT OF BeO BLOCK WINDOW REFERENCED TO PLANE Y WITH LOAD IRIS IN PLACE	20
13	BROADBANDED BeO BLOCK WINDOW CHARACTERISTICS SHOWING MEASURED AND COMPUTED GHOST MODE	21
14	DIMENSIONAL DRAWING OF BeO BROADBAND WINDOW	23
15	THERMAL FAILURES OF TWO AL995 HALF-WAVELENGTH BLOCK WINDOWS.	24
16	THERMAL FAILURES OF HALF-WAVELENGTH BLOCK AL300 AND AL399 WINDOWS	25

LIST OF ILLUSTRATIONS, (cont.)

Figure		Page No.
17	POWER DISSIPATION IN AL300 HALF-WAVELENGTH BLOCK WINDOW	26
18	POWER DISSIPATION IN AL995 HALF-WAVELENGTH BLOCK WINDOWS	27
19	COMPONENTS OF WINDOWTRON ASSEMBLY	29
A-1	DOUBLE DISC WINDOW MODEL SHOWING MATRIX DESIGNATIONS	34

SECTION I

OBJECTIVES OF PROGRAM

1-1. INTRODUCTION

This report is the third of four quarterly technical notes and one final technical report to be prepared for Rome Air Development Center, Griffiss Air Force Base, New York. Varian Associates of Palo Alto, California, is conducting this study for the United States Air Force under Contract Number AF 30(602)-2844. This contract, awarded 6 July 1962 in accordance with RADC Exhibit "A," dated 29 December 1961, is entitled "High Power R-F Window Study."

1-2. OBJECTIVES

A. Primary

The objectives of the High Power R-F Window Study are to conduct theoretical and experimental investigations of methods for improving the average power handling capabilities of high average power microwave tube windows. The final objective is to design and test an X-band window with 25 per cent bandwidth up to at least 250 kilowatts of c-w power.

In the pursuit of the final objective various phenomena believed to be responsible for window failure in the field and under operating conditions will be investigated. These include effects of multipactor, stray magnetic fields, variations of gas pressure and the relative merits of various gaseous or liquid dielectrics used for cooling of double disc windows.

An investigation of various solid dielectrics, with respect to their adaptability and desirability for use in configurations best suited for high average power transmission, will also be made.

B. Third Quarter Objectives

Retesting of all previously successfully tested windows, particularly the beryllium oxides, had been scheduled for this quarter. These windows were to have been connected by means of a flange with O-ring to a sapphire window so that the volume between the two windows could be evacuated and used as a windowtron. This combination was necessarily unbakeable because of the O-ring, and thus high outgassing was experienced under high power.

This type of windowtron was abandoned early in the quarter in favor of building a completely bakeable assembly, which is now complete.

High power testing of a series of AL300, AL399 and AL995 half-wavelength block windows was scheduled and has been completed. The object was to compare these results with the results of identical high power tests performed on beryllium oxide windows. Such windows, if able to withstand up to 250 kilowatts in a nitrogen pressurized atmosphere, were also scheduled to be retested in the windowtron. As it turned out, all of the alumina ceramic block windows fractured at or near 100 kilowatts cw (test frequency $\cong$ 7750 Mc.).

Further development of the double-disc type of window configuration was also scheduled for later during the third quarter. Several versions of this window are now ready for fabrication using AL300 and AL400 ceramics. One full-wavelength, 10 per cent bandwidth double disc window was completed and is now awaiting windowtron tests.

Investigation into the possible improvement of the resonant ring tuning mechanisms was programmed for the third quarter. After several new methods of accomplishing this tuning were attempted and reasons for breakdown examined, it was concluded that a near perfect match must be attained within the circuit for optimum trouble-free performance. Several modifications on the ring circuit have been made as a result.

Broadbanding of both the half-wavelength block and thin disc windows was scheduled for the third quarter and is discussed in more detail in the main body of the report. Broadbanding of windows by analytical means with the use of a computer was not originally scheduled for this period but as a result of much laboratory effort, it was felt that an analytic approach would be useful. This was pursued to some extent and is reported herein.

SECTION II

TECHNICAL PROGRESS OF PROGRAM

2-1. GENERAL DISCUSSION

A. Conferences

On the 5th and 6th of February, 1963, Mr. Dirk Bussey, Rome Air Development Center's contract engineer visited Varian Associates' laboratories in Palo Alto to appraise contractual progress and to attend the High Power Microwave Window Seminar for which Varian Associates acted as host. This seminar was sponsored jointly by the Department of Defense, Advanced Research Projects Agency, and the U. S. Army Electronics Research and Development Laboratories.

A paper reviewing the results of the "High Power R-F Window Study" written by Mr. F. O. Johnson and Mr. J. D. Miller was presented by Mr. Miller at this seminar.

B. Window Synthesis by Computer Solution

In the design of windows for particular applications, much thought is usually given to the configuration best suited to that application. The deciding factors are usually bandwidth required, cost or ease of manufacture, size and proven power handling capability. Once a type of window has been chosen for more detailed design work, it becomes necessary to cold test in order to minimize the reflection coefficient across the band of frequencies desired.

In some cases the dimensions of the window can be estimated quite accurately from previous experience with similar windows. However, in many cases a considerable number of cut-and-try experiments must be performed before a satisfactory result is obtained. What is needed, then, is a model for the window which can be described mathematically. The resulting mathematical expression could be programmed for computer solution, and by varying dimension, dielectric constant and frequency dependent parameters, many experimental windows could be verified in a short time. Thus, simulating cold test experiments with the computer would be a powerful tool in window circuit optimization.

A desirable feature of a programmed solution is that it could be used for a wide variety of window configurations. Two such configurations are shown in Figure 1. All that is necessary is the ability to define in mathematical terms the contribution of each of the components of the window assembly. In most cases these components will be limited to irises, lengths of waveguide (dielectric or air loaded), dielectric interfaces and transitions from one size or form of waveguide to another.

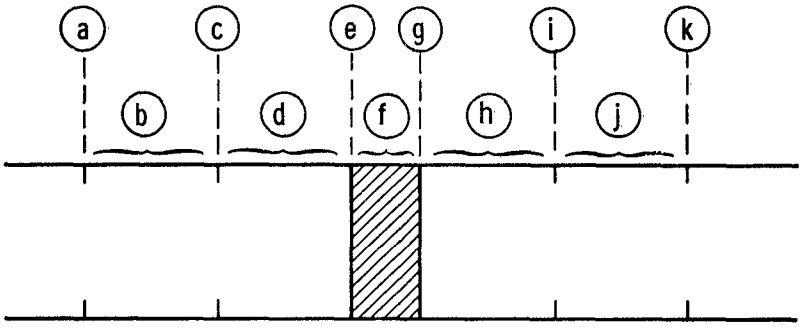

(a) Half Wavelength Block Window With Cascaded Broadbanding Irises

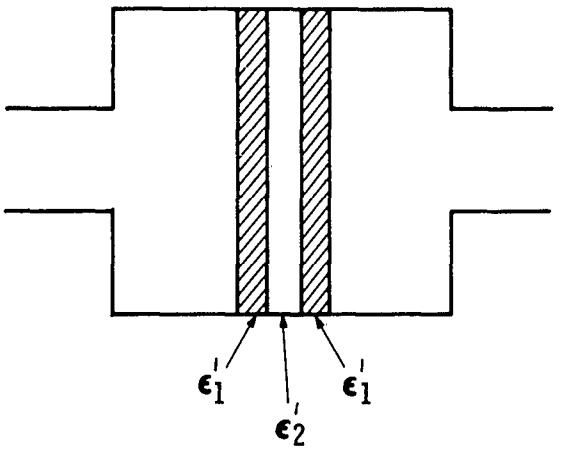

(b) Double Disc Fluid Dielectric Cooled Window

FIGURE 1
WINDOW CONFIGURATIONS

Scattering matrices[1] are easily used to define the components and are in turn readily redefined as transmission parameters.[2] For example, in the upper sketch of Figure 1 there are eleven component matrices between the indicated planes (a) and (k). In planes (a), (c), (i), and (k) are shunt susceptances. Planes (e) and (g) contain interfaces between two dielectrics. Regions b, d, f, h, and j are transmission line sections where f is dielectrically loaded. The window sketched in Figure 1(b) can be handled similarly, including a matrix for the transitions between waveguide sizes. The definition and/or derivation of each of the transmission matrices is shown in the Appendix, along with the final result which is

$$\left[T\right] = \left[T^a\right]\left[T^b\right]\left[T^c\right] \quad \ldots \quad \left[T^i\right]\left[T^j\right]\left[T^k\right] \tag{1}$$

where

$$T = \begin{bmatrix} T_{11} & T_{12} \\ T_{21} & T_{22} \end{bmatrix} \tag{2}$$

The composite window can be represented as shown in Figure 2. It is demonstrated in the Appendix that

$$b_2 = T_{11}\, a_1 + T_{12}\, b_1 \tag{3}$$

$$a_2 = T_{21}\, a_1 + T_{22}\, b_1 \tag{4}$$

where

a_1 is the incident wave at the input

b_1 is the reflected wave at the input

a_2 is the incident wave at the output

b_2 is the reflected wave at the output

If the window network is terminated in a reflectionless load, a_2 will be zero. Therefore, from Equation 4

$$\frac{b_1}{a_1} = -\frac{T_{21}}{T_{22}} = \rho$$

or

$$|\rho| = \left|\frac{T_{21}}{T_{22}}\right|$$

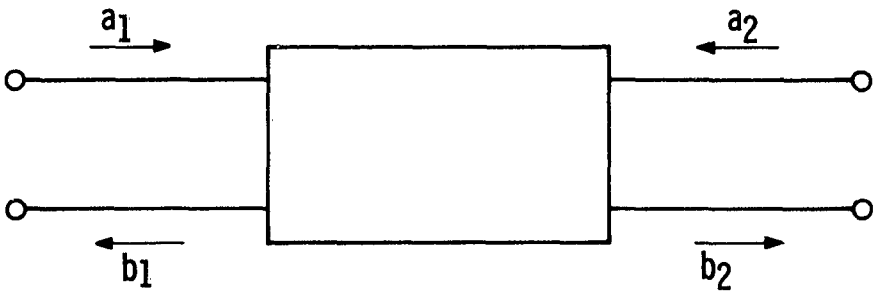

FIGURE 2
FOUR TERMINAL NETWORK REPRESENTATION
OF A WAVEGUIDE WINDOW

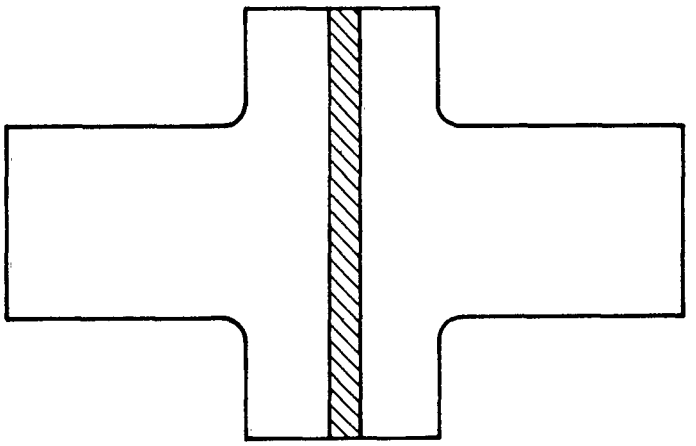

FIGURE 3
SYMONS-TYPE THIN DISC WINDOW

or

$$\text{VSWR} = \frac{1 + \left|\frac{T_{21}}{T_{22}}\right|}{1 - \left|\frac{T_{21}}{T_{22}}\right|} \tag{5}$$

Equation 5 represents the desired information from the solution so that it can be plotted versus one of the other variables, such as frequency.

During the last portion of this reporting period, Equation 1 was programmed in the Fortran II language. The window selected for initial computer solution is shown in Figure 3. It is a simpler version of the one shown in Figure 1(b).

In order to define matrices a and k, which come about as a result of abrupt transition from rectangular to cylindrical waveguide, open circuit, short circuit and terminated impedances were measured[1] for the frequency band of 7.0 to 10.0 kMc at 0.2 kMc intervals. In this way z_1, z_2, z_3 are defined as the terminated, short circuit and open circuit impedances, respectively, all normalized to the characteristic impedance of the input waveguide. Figure 4 shows a cross-sectional view of the test setup used to measure these impedances.

Since this is an abrupt transition, fringing fields probably set up several evanescent modes which could abrogate any measurements made of the transition impedances. Therefore, in an effort to reduce the effect of these modes, a reference plane was chosen at plane A of Figure 4 which is far enough away from the transition.

Several debugging runs were required for the program. This is not unusual considering that the matrices are all written in complex numbers. As a check on the final debugging run, one case was hand calculated. Complete correlation was achieved by this method.

Before the writing of this report, time permitted computation of only one complete set of results for the window of Figure 3 and for one set of parameters. The results were conclusive enough to show that an error exists either in the measurement of the abrupt transition impedances or in the mathematical model.

It is anticipated that during the next quarter work will be continued to improve the definition of the model and the result will be an additional powerful tool for use by window designers.

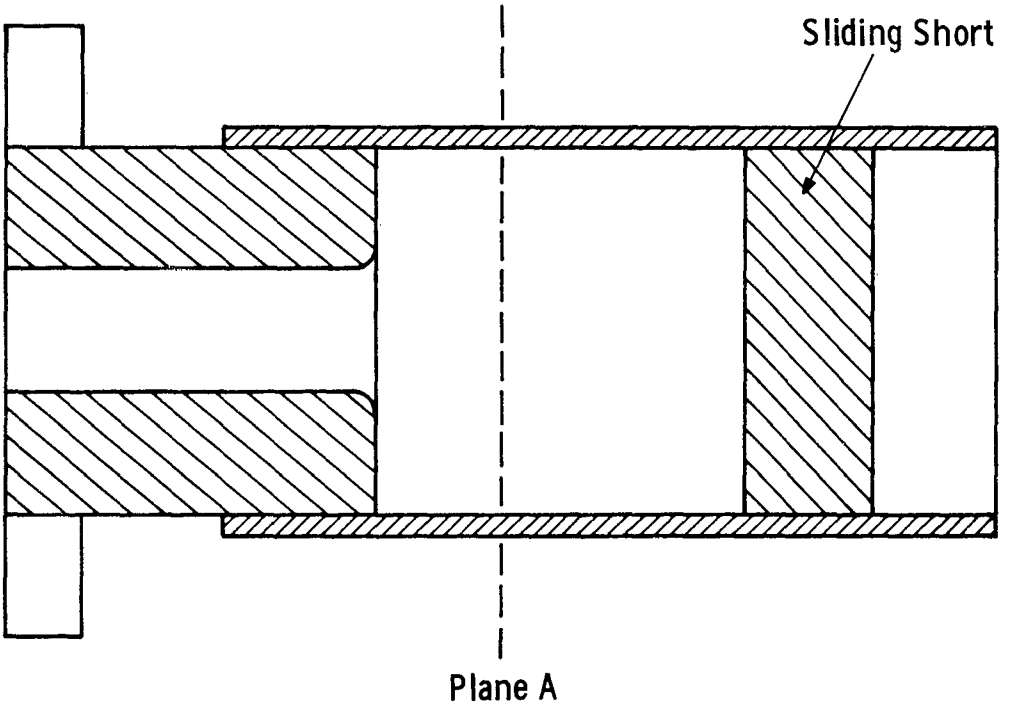

FIGURE 4
CROSS SECTION OF TEST JIGS USED TO MEASURE
TRANSITION PARAMETERS z_1, z_2, AND z_3

2-2. WINDOW CONSTRUCTION AND HIGH POWER TESTING

A. Single Thin Disc Fused Quartz Windows

Considerable effort directed toward high power testing of single thin disc fused quartz windows has shown, as reported in Quarterly Technical Note No. 2, that this material gets extremely hot when subjected to multi-kilowatt power levels.[3] In fact, all commercial grade fused quartz windows tested prior to the third quarter failed quite conclusively.

In an effort to determine whether there is any variation in materials between manufacturers, and if minute bubbles, contained in all but the most perfect quartz specimens, are a cause of these failures, several samples of grade A optical fused quartz were obtained from the Amersil Company. The trade name of this 100 per cent bubble-free material is Homosil.

The vehicle for testing these samples is the Symons-type pillbox window exactly as sketched in Figure 2 of Quarterly Technical Note No. 2. This window using "Homosil" performed somewhat better than the previously tested, mechanically identical models. At a power level of 163 kilowatts cw, the nitrogen atmosphere of the resonant ring again ionized. An increase in pressure eliminated that problem. At 190 kilowatts cw a portion of the quartz discs face began to glow with an orange color. This color has been characteristic of the quartz as it begins to melt. Further increase in power to 210 kilowatts caused only a slight brightening of the glow. Repeated backing off and increasing the power over the 175 to 210-kilowatt range verified the 190 kilowatt level as being the apparent softening point of that sample.

After this test the sample was examined under ordinary and polarized light but no melted areas or strains were seen. It is felt that because there was no pressure differential in the axial direction of the window, no deformation of the quartz occurred. Perhaps the better grade of quartz is responsible for this superior performance as compared to previous samples. On the other hand, fused quartz does not appear to offer much help in high power window applications because it gets so extremely hot.

Figure 5 illustrates the power dissipated as a function of power transmitted for the window discussed above.

B. Single Thin Disc Sapphire Windows

Both samples of zero degree cut synthetic sapphire shown in Figures 12 and 13 of Quarterly Technical Note No. 2 have been brazed into window housings. The final assembly (see photograph of Figure 6 and VSWR characteristics of Figure 7) of one of them is completed and is vacuum tight.

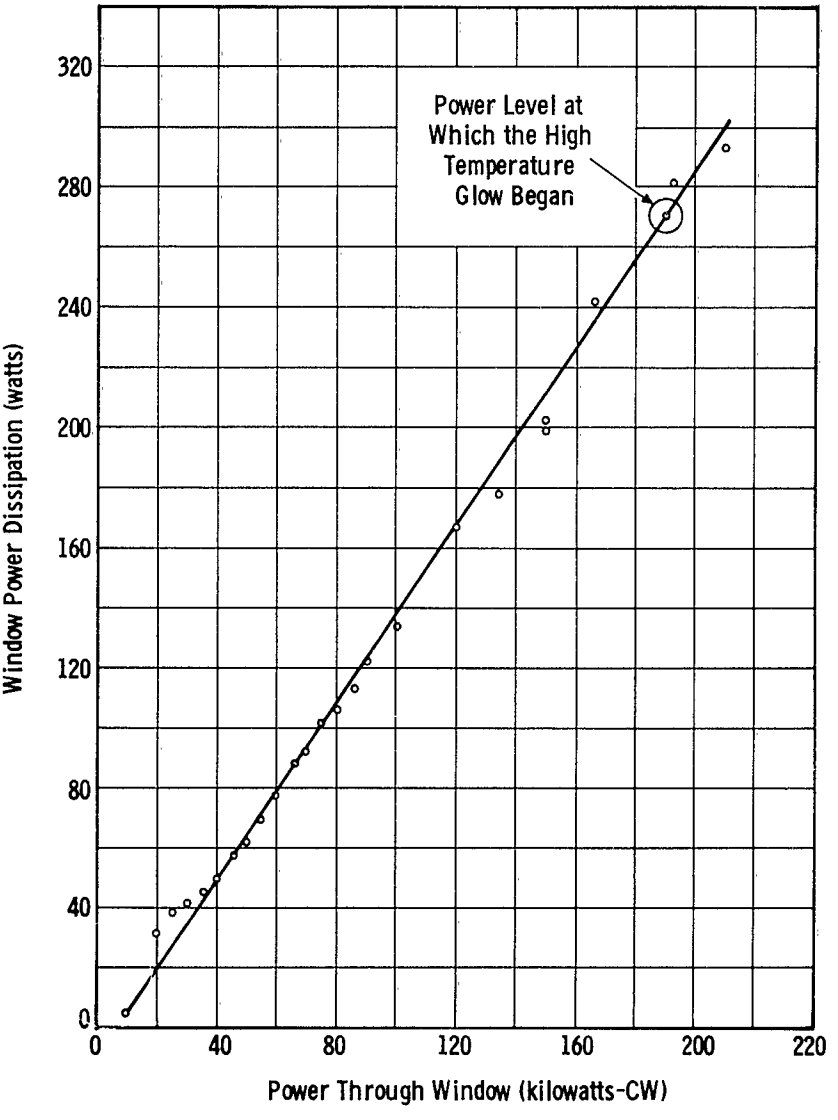

FIGURE 5
POWER DISSIPATION
IN QUARTZ THIN DISC WINDOW

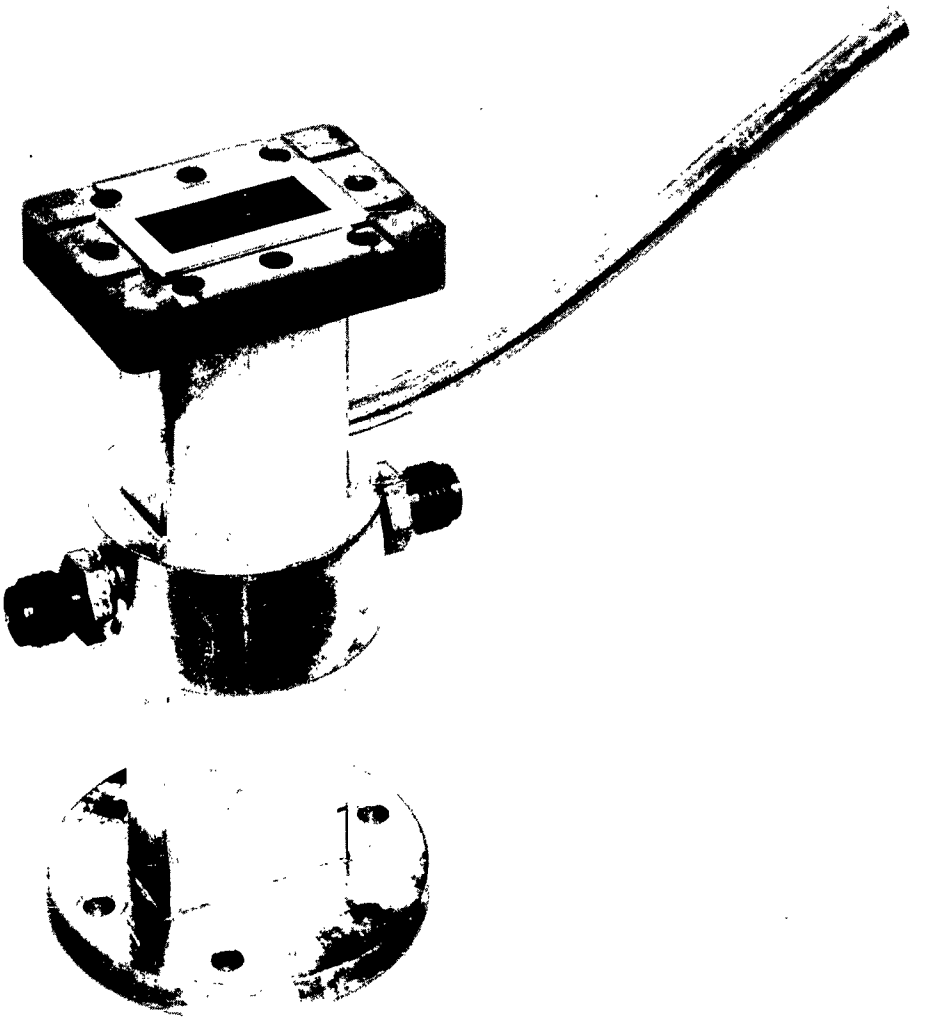

FIGURE 6
SINGLE DISC SAPPHIRE WINDOW ASSEMBLY

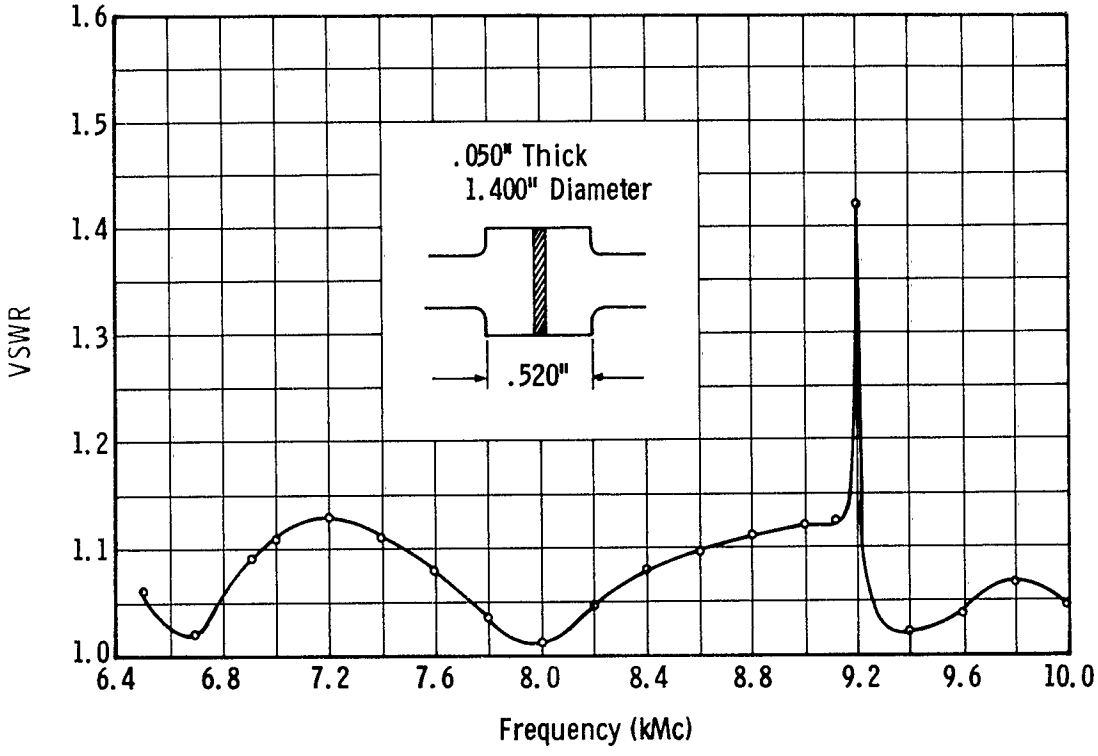

FIGURE 7
SINGLE DISC SAPPHIRE WINDOW CHARACTERISTICS

Unfortunately the bonding braze on the second disc did not hold and successive attempts to rebraze it failed. The only alternative at this point is to regrind the edges and redo the metallization and brazing operations. It had been hoped that a comparison between sapphire windows with the boule seed at the center and off-center of the discs could be made. If the second disc, whose boule seed is at the center, is salvagable, then the comparison will still be made.

The assembly of Figure 6 is completely bakeable and is intended for use as part of a windowtron which will be discussed later.

C. Double Thin Disc Windows

During the last reporting period, two double thin disc windows were completed and tested. Because the power transmitted by one of them was an acceptable 180 kilowatts, fabrication of more assemblies was temporarily halted in favor of completing some of the work on other types of windows.

Just recently another version of the double disc window using AL300 has been completed. A photograph of it is shown in Figure 8. Four tubing attachments can be seen and it should be pointed out that two of them cool the outside jacket with water while the center two allow cooling by gaseous or liquid dielectrics.

This window does not have the bandwidth stated in the objectives of this program, but it does have advantages which might make it desirable for less broadband applications. Electrically it is approximately one full wavelength long, putting the ceramics closer to an electric field minimum as well as moving them away from the rectangular to cylindrical waveguide transitions. The window thicknesses are also each fully as thick as need be for a single disc window of this diameter. These two factors alone will provide much in the way of power handling capacity despite the fact that the bandwidth is reduced to 9.5 per cent, as shown in Figure 9.

This assembly is also completely bakeable and is intended for use as the other half of a windowtron in conjunction with the sapphire window.

Several discs of AL400 ceramic are in the process of being fired and machined for use in some thin double disc assemblies similar to those previously reported on. The difference will be an increased thickness which will improve mechanical strength.

D. Half-Wavelength Beryllium Oxide Windows

1. High Power Test

One assembly using National Beryllia's high density beryllium oxide body was tested to 222 kilowatts cw without failure. This window was cut to be one

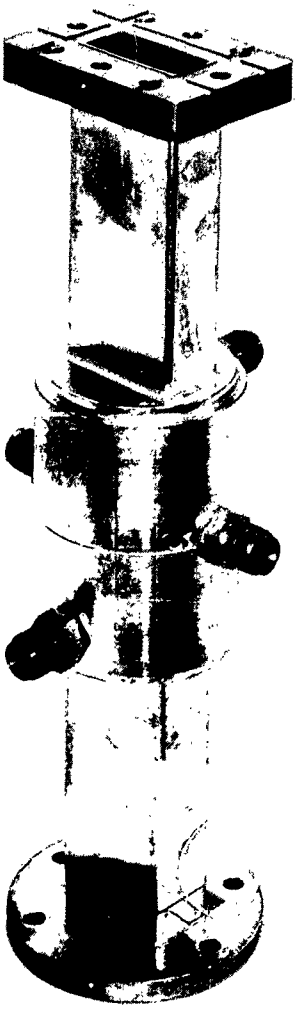

FIGURE 8
DOUBLE DISC AL300 WINDOW ASSEMBLY

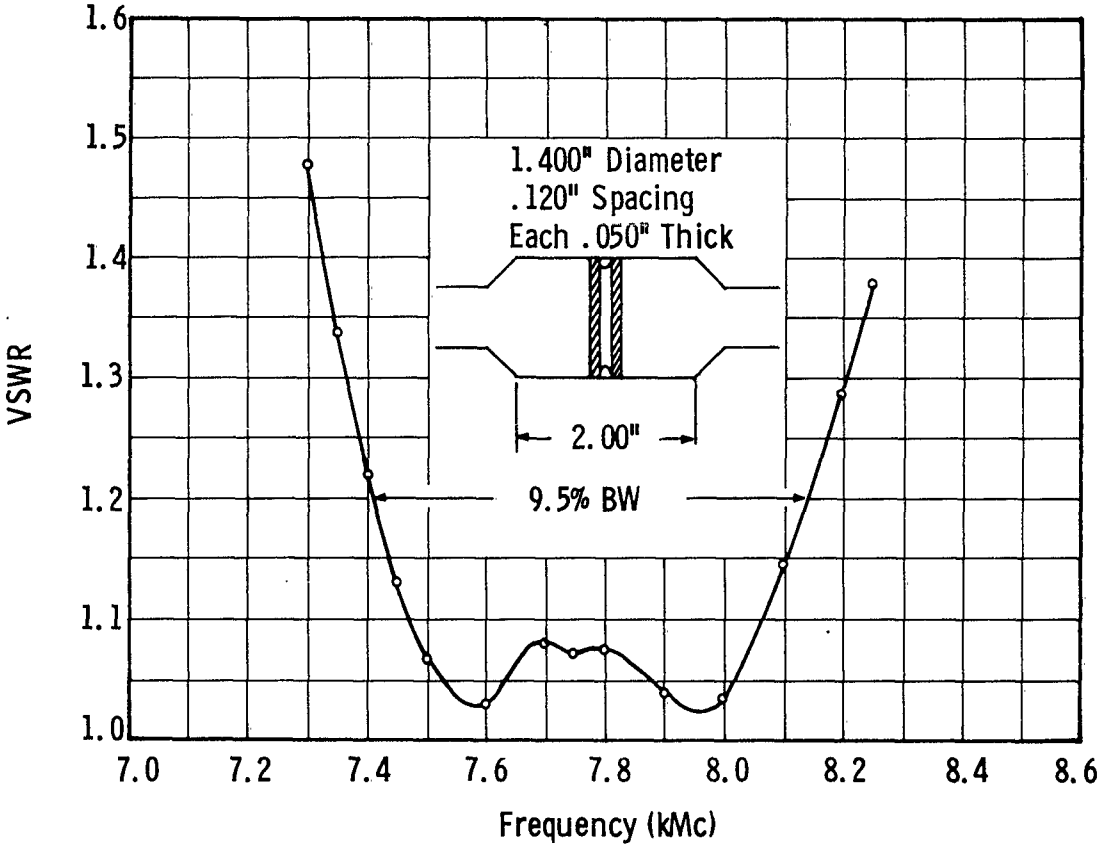

FIGURE 9
DOUBLE DISC AL300 WINDOW CHARACTERISTICS

half-wavelength long at 7750 Mc and was fabricated and tested to compare with the previously tested Brush beryllium oxide.

The power dissipation versus power transmitted through the window is shown in Figure 10. This material appears to dissipate 10 to 40 per cent less power than the beryllias previously tested. Tests were discontinued because of breakdown in the resonant ring tuners.

2. Broadbanding of Beryllium Oxide Windows

The substantially high average power handling capability of the beryllium block window reported as a result of this window study program has provided the motivation to investigate the broadband possibilities of such a window material and geometry. The problem of broadbanding the planar block waveguide window has been extensively investigated by Staprans and Mercer,[4] Churchill,[5] and several others. It is possible to write an analytic set of equations, derived from transmission line and filter theory considerations, to describe a window assembly in terms of the ceramic and any other arbitrary linear, passive matching elements.

Such an approach in general leads to a set of transcendental or otherwise cumbersome equations which often take longer to solve analytically for a specific design than to obtain similar results by judicious use of the Smith impedance plot.[5]

The bandwidth of a beryllium oxide block window similar to those which have successfully handled c-w power of 250 kilowatts can be substantially increased by the procedure described below.

First, a "mode search" was made for a BeO block geometry in the frequency band of interest. By inspecting a mode frequency versus aspect ratio computation similar to that shown in Figure 20 of Quarterly Technical Note No. 2, an aspect ratio was chosen to give reasonable mode clearance for as high a guide height (lower field gradient) as possible. For a beryllium oxide block with relative dielectric constant of 6.5 and cut to operate at 7750 Mc, computation of the first order even modes showed that the bandwidth available was better than 13 per cent using an aspect ratio of 1.9. Normal aspect ratio of WR 112 waveguide is 2.26. The range of frequencies over which mode clearance was precalculated was from approximately 7.6 to 8.6 kMc. Ordinarily the block would be cut to be $\lambda g/2$ at the center of the mode free band and then broadbanded. For the purposes of this program, though, 7750 Mc was better because that is the high power test frequency. The broadbanding procedure is not altered by this deviation. Since power must enter and leave the window in standard height guide, 19 per cent tapers were constructed. The added reflection of these nominal tapers is negligible, for they are on the order of one half-wavelength long. In cases demanding even smaller aspect ratios, the taper reflections can be minimized by choosing the proper taper length.[6]

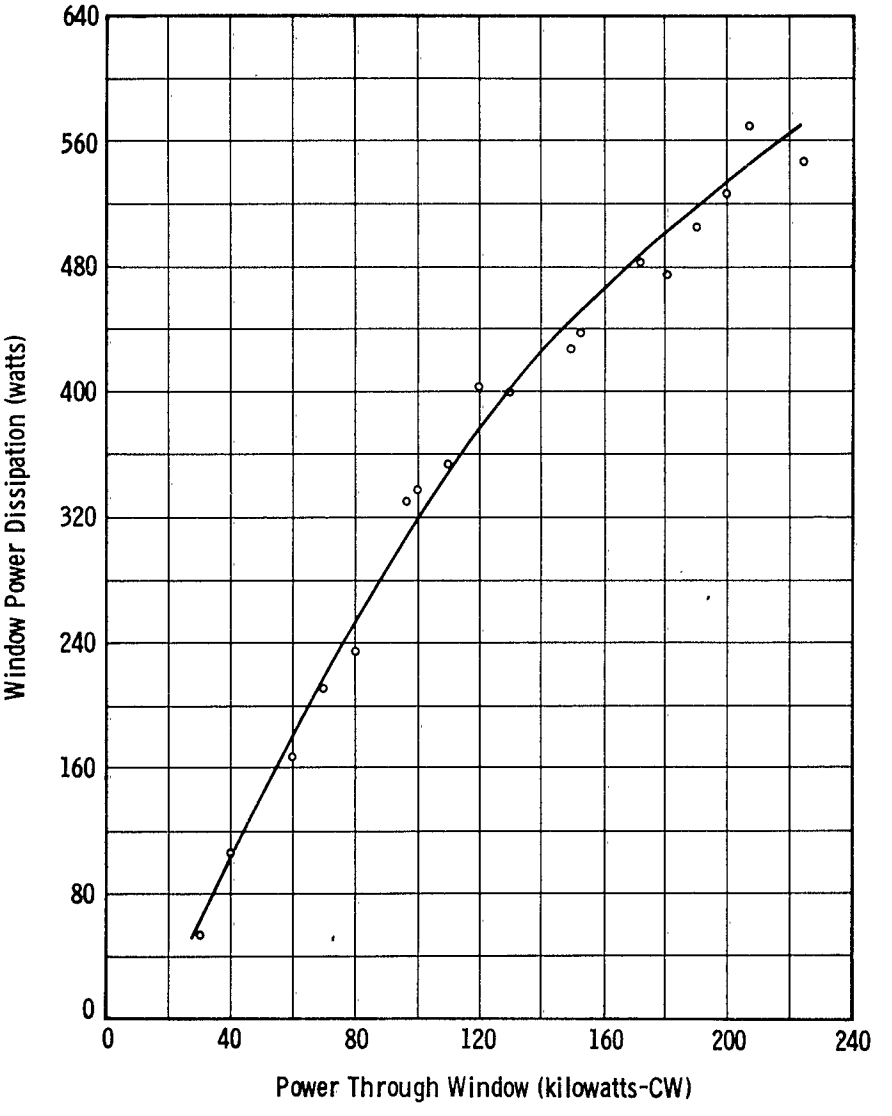

FIGURE 10
POWER DISSIPATION IN NATIONAL BERYLLIA
HIGH DENSITY BeO BLOCK WINDOW

Since only the height of the window has been increased by a single taper, thus not altering the guide wavelength, no problem was encountered in determining the impedance function arbitrarily close to the window face. This, of course, is necessary in order to determine the position and magnitude of the shunt susceptances needed.

By terminating one end of the window with a flat load, the Smith plot admittance function of the window was determined in the conventional way with slotted line. This admittance function was then referenced to a point approximately three-eighths of a guide wavelength from the source window face so that the function closely approximates a circle lying symmetrically on either side of the purely positive imaginary ordinate. See curve A of Figure 11.

The point at which this admittance circle goes through the origin of the Smith plot is, of course, the frequency at which the window is resonant, or a half-wavelength long.

Now it is readily seen that a properly chosen lumped inductive element at plane X would move the greater part of the admittance circle into a path concentric with the origin of the Smith plot. Indeed, as a 0.37 normalized inductive susceptance was added on plane "X," the curve labeled as B in Figure 11 was the result. The window with a single pair of irises now presents a constant VSWR of approximately 1.45 over a wide frequency band.

It is now possible to argue from the reciprocity theorem that reversing incident and terminal sides of the composite structure will not change the observable VSWR. Since impedance points of constant VSWR may be closed by moving toward the load (on the Smith plot high frequency points move faster than low frequency points because of smaller λg), it is expected that the admittance circle points around the origin can be found to cluster at some reasonable distance from the window. In fact it is intuitively felt from symmetry, and empirically shown here, that the distance for clustering is exactly the distance from the window of the first iris. Since a filter network was anticipated in the beginning, this admittance cluster would again be expected to fall on the purely positive imaginary susceptance ordinate. See Figure 12.

A 0.38 normalized susceptance moves the admittance cluster to the origin of the Smith plot, and broadband matching has been achieved as shown in Figure 13.

If minimum mismatch is desired over the widest mode-free region (i.e., between the TM_{11} and TM_{21} modes) a minor shifting of the inductive irises will cause the match to improve at the high end of the band without degrading the center frequencies appreciably. This can be deduced from a study of Figure 11, curve B. With these adjustments, a mode-free bandwidth of 13 per cent could be obtained with a maximum VSWR of 1.05.

(1) 7.4 kMc
(2) 7.8 kMc
(3) 8.4 kMc

A. Referenced to Plane X
B. Inductive Susceptance of 0.37 Added at Plane X

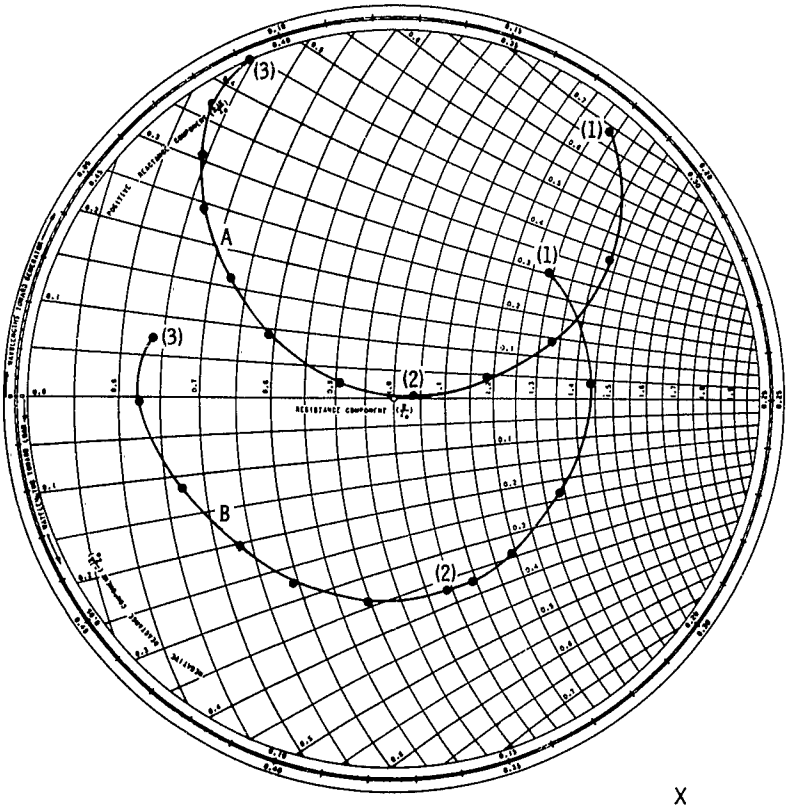

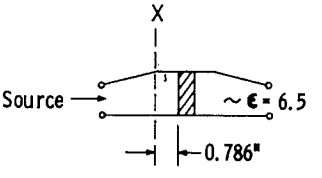

FIGURE 11
ADMITTANCE PLOTS OF X-BAND BeO BLOCK WINDOW

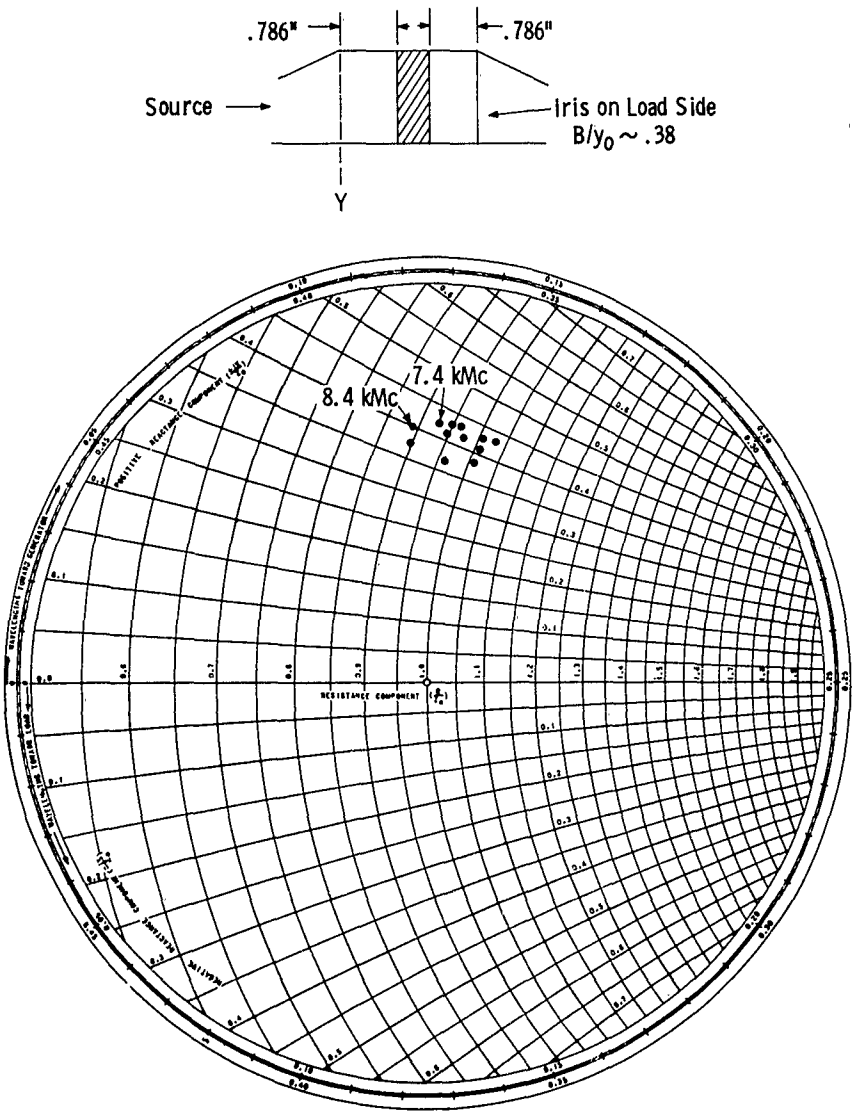

FIGURE 12
ADMITTANCE PLOT OF BeO BLOCK WINDOW
REFERENCED TO PLANE Y WITH LOAD IRIS IN PLACE

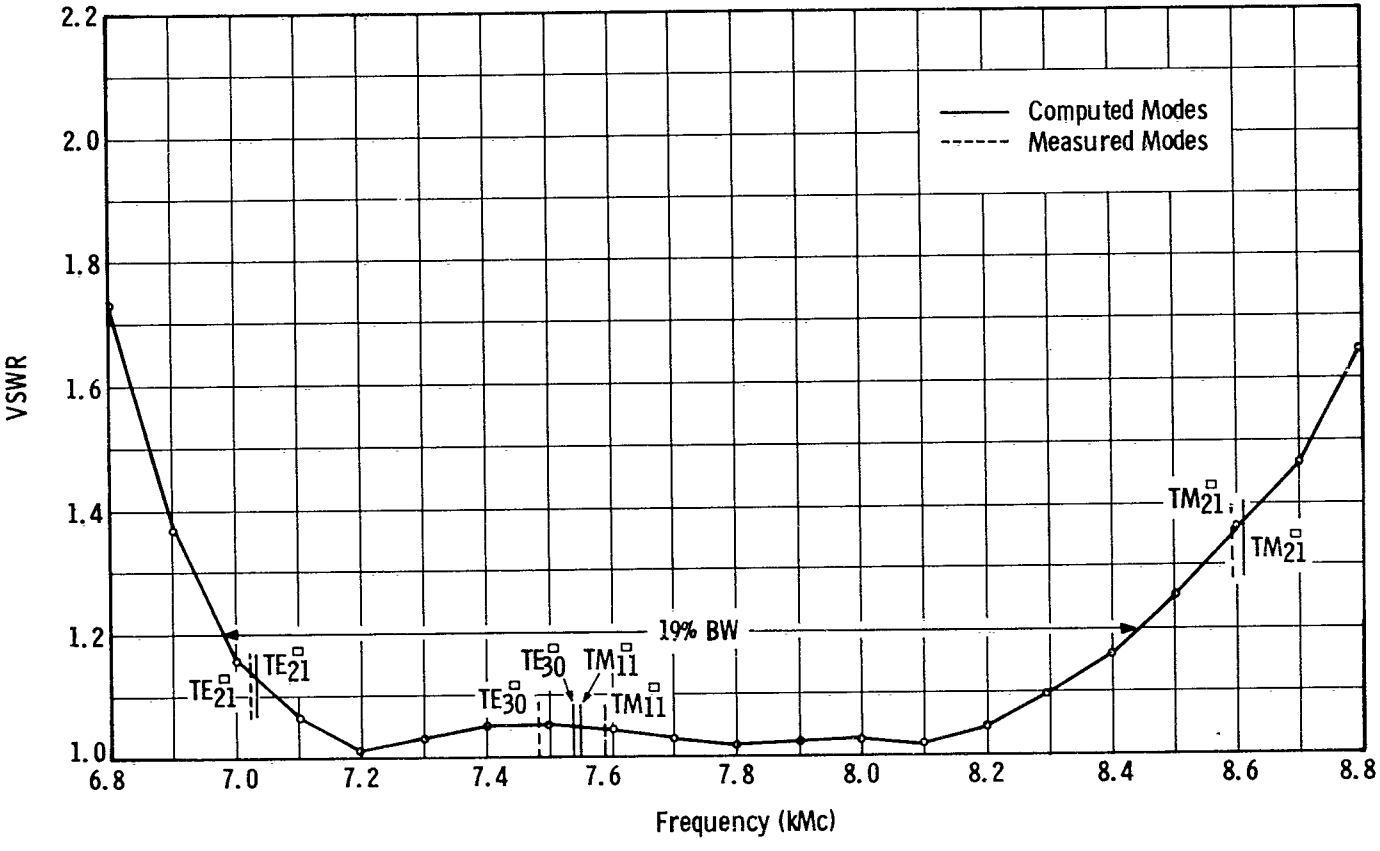

FIGURE 13
BROADBANDED BeO BLOCK WINDOW CHARACTERISTICS
SHOWING MEASURED AND COMPUTED GHOST MODE

The final broadband window dimensions are shown in Figure 14.

Since matching irises, as large as 0.2 normalized susceptance, have been successfully used on beryllia windows carrying up to 250 kilowatts of c-w power in the resonant ring, power testing of the described broadband BeO window will not be pursued at this time. However, should time permit toward the end of this program, an effort will be made to perform such tests. As of now it suffices to say that the availability of large mode-free bandwidths for high c-w power windows has been demonstrated.

E. Half-Wavelength Aluminum Oxide Windows

Several aluminum oxide half-wavelength block windows have been tested in the resonant ring during this past quarter and all have failed from what appears to be thermal heating. Photographs of these failures are shown in Figures 15 and 16. The cracks consistently appear near the center of the block much as would be expected considering that this is in the highest power density region.

The particular windows tested were made from AL300, AL995, and AL399, as indicated. For those readers not familiar with AL399, it is a 99.0 per cent pure AL_2O_3 body with a loss tangent of 0.00021 (100° C - 8.5 kMc) and a dielectric constant of 9.61 (25° C - 8.5 kMc). It is a material with only slightly different properties and only slightly less pure than AL995, which is a fairly well-documented product.

In the interest of saving time, all of the block samples were not broadbanded but simply cut to be $\lambda g/2$ at the test frequency of 7750 Mc. In this way it was only necessary to use (in some cases) small trimming irises for producing a perfect match at the test frequency.

Power dissipation curves are shown in Figures 17 and 18 for AL300 and AL995, respectively. The power levels at which failure occurred in each case are indicated, but with some reservation as to the exact point. Because of the absence of visible effects such as arcing when breakdown occurs, and because the tests were performed with both faces of the window pressurized, the exact power level at which the ceramic cracked cannot be determined. As a result of this lack of failure indicators, the experimental procedure was to remove the test windows for examination every time power was increased 20 or 30 kilowatts. By this method only the range of power levels at which failure occurred can be determined.

One conclusion can be drawn from all of the experiments and tests with block ceramic windows. Aluminum oxide windows in WR 112 waveguide will generally fail at or below 100 kilowatts cw. Beryllium oxide block windows in identical configuration and waveguide will take more than 250 kilowatts cw. The upper limit of this material is still now known and will not be known until a much higher power resonant ring is built.

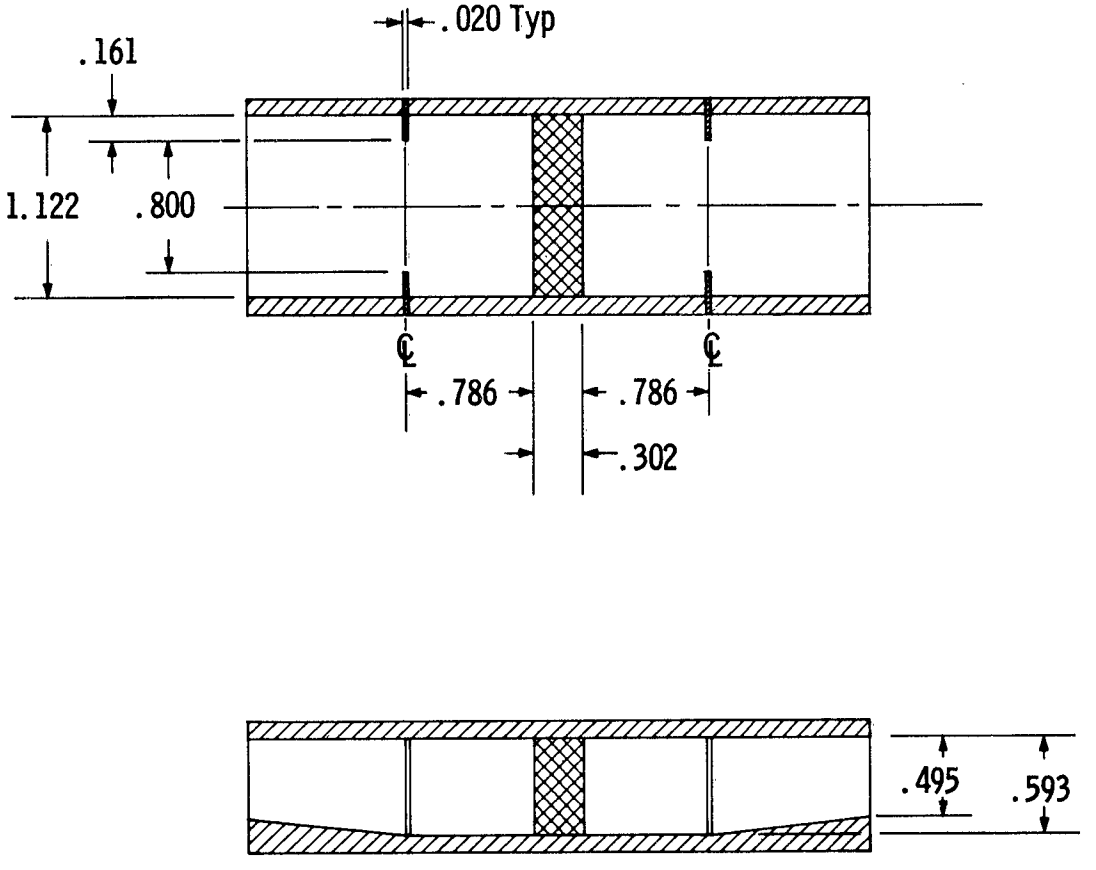

FIGURE 14
DIMENSIONAL DRAWING OF BeO BROADBAND WINDOW

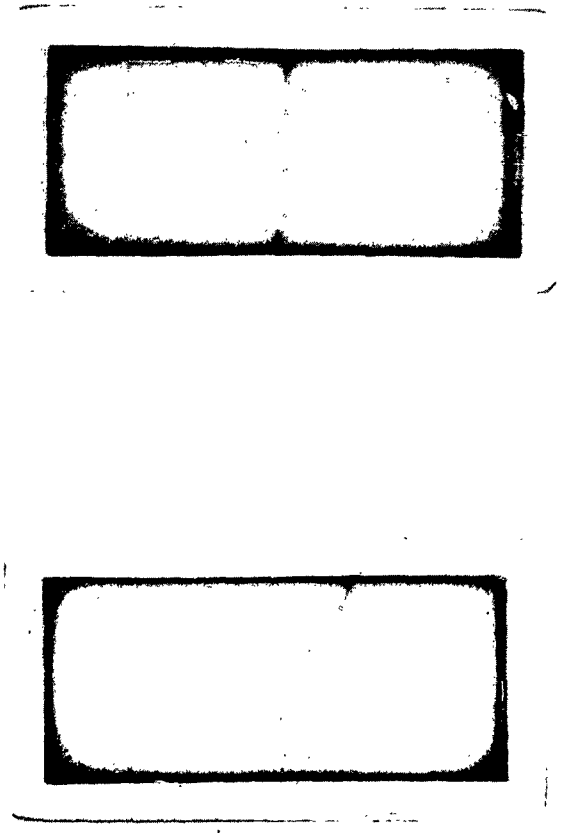

FIGURE 15
THERMAL FAILURES OF TWO AL955
HALF-WAVELENGTH BLOCK WINDOWS

(a) AL300

(b) AL399

FIGURE 16
THERMAL FAILURES OF HALF-WAVELENGTH
BLOCK AL300 AND AL399 WINDOWS

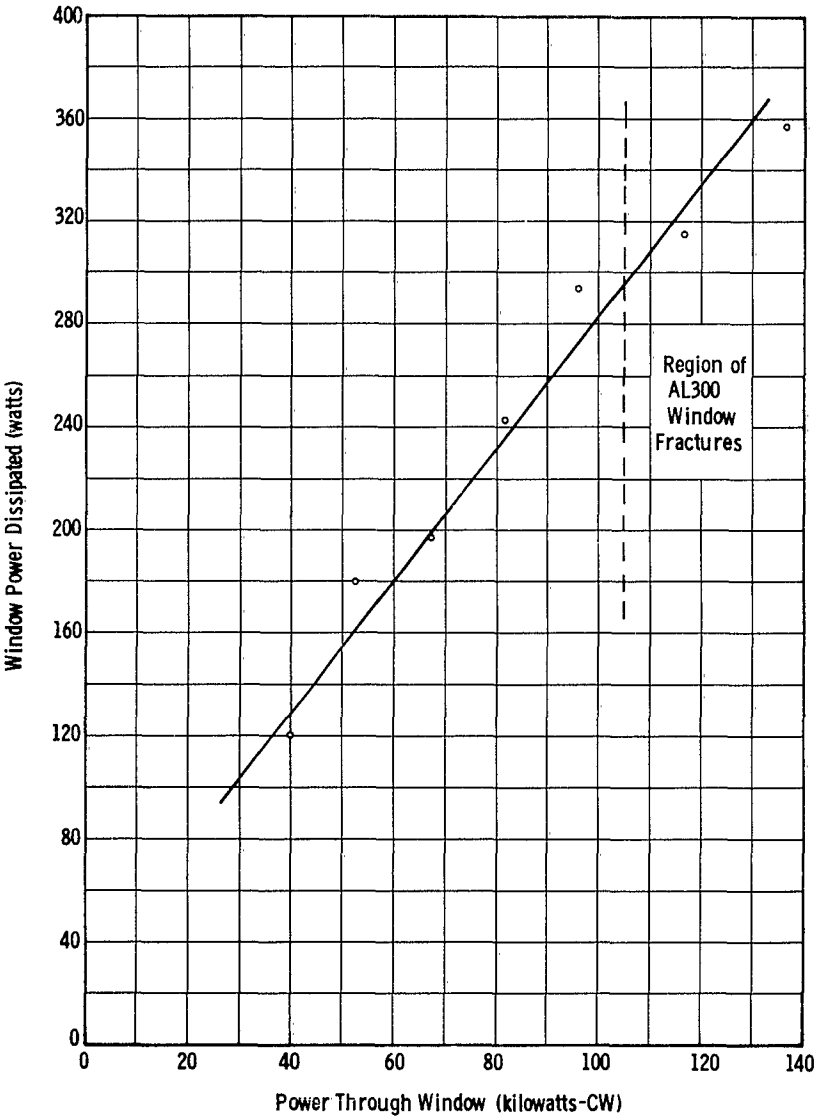

FIGURE 17
POWER DISSIPATION IN AL300 HALF-WAVELENGTH
BLOCK WINDOW

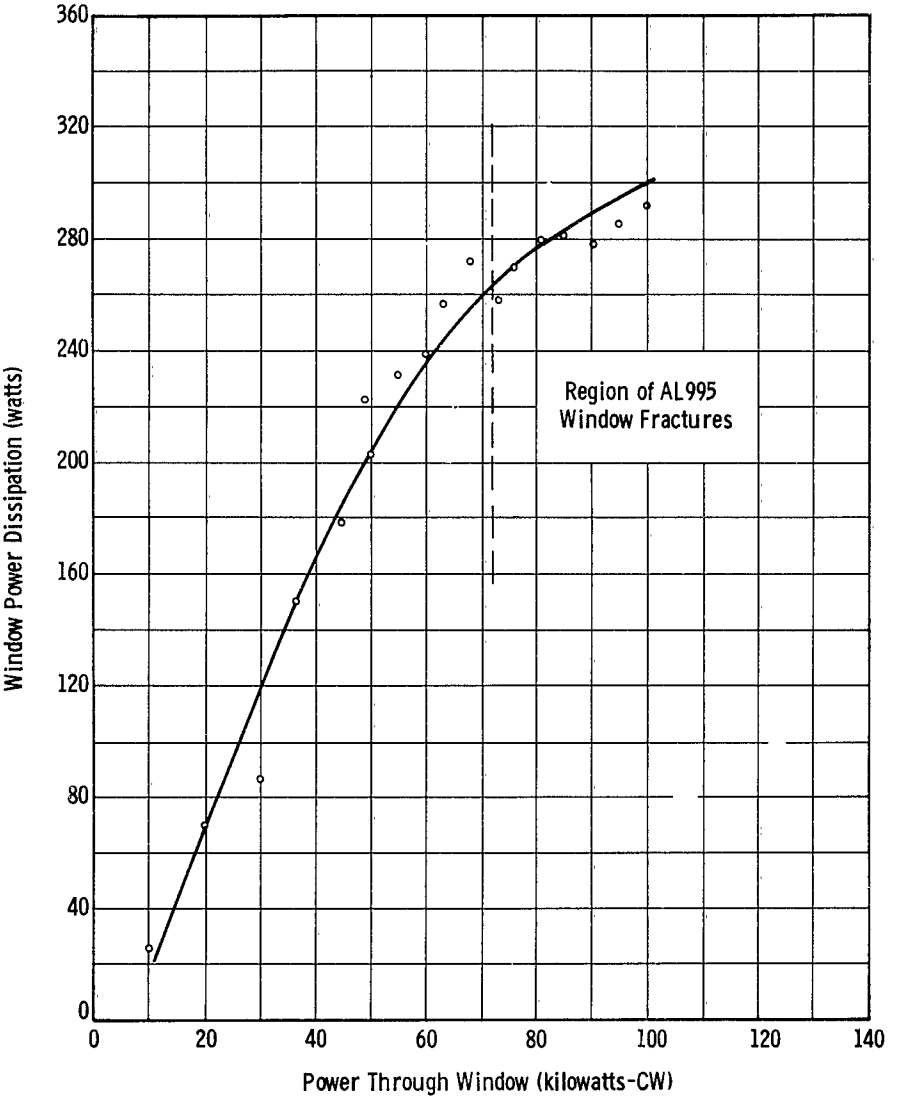

FIGURE 18
POWER DISSIPATION IN AL995 HALF-WAVELENGTH
BLOCK WINDOWS

F. Windowtron Resonant Ring Testing

As indicated in previous sections of this report, high power testing with pressurized gases on both sides of the window has not been entirely satisfactory even though much information has been gleaned from the numerous tests performed. One disadvantage is that it does not permit simulation of actual tube operation conditions, i.e., a vacuum on the power input side of the window. Neither can a study of multipactor be made without a vacuum. Therefore, high power tests were attempted on a windowtron composed of a sapphire window and a beryllium oxide window. Both of these had been tested to 250 kilowatts cw independently. These two windows were joined by a flange and O-Ring combination whereby a vacuum of 10^{-5} to 10^{-6} Torr was obtained. A one liter VacIon was used to continuously pump the region between the windows. Successive attempts at raising the transmitted power through this device to values above 20 kilowatts failed because of continuous outgassing of the system. Part of the trouble was also attributed to the flange and O-Ring combination which became quite warm even at these relatively low power levels.

These tests were discontinued and the apparatus discarded in favor of designing a new and bakeable windowtron, a part of which could be used for many tests. Figure 19 is a photograph of the new windowtron and its components. The sapphire disc and double disc assemblies previously discussed are shown and are to be attached to one another by means of a vacuum tight flange and gasket and continuously pumped with a 5 liter VacIon pump.

This type of flange is a proven device used in Varian Associates evacuated S-Band ring with very good results. Losses in this type of flange connection are considerably less than in any other flange tested. Heating effects will then be greatly minimized. The flange is also bakeable and is reusable simply by inserting a new gasket.

It is expected that the sapphire window will be used as one half of the windowtron for all of the windowtron tests. In this way the evacuated power input side of the window under test can be viewed through the transparent sapphire, and the power output side can be viewed through the viewing port on the other end. Both viewing ports, designed into the 180° bends, are also shown in Figure 19.

Because of past difficulties with even small mismatches present in the resonant ring, each individual component of the ring has been individually nearly perfectly matched by small inductive irises. If a near 1.0 VSWR has been achieved it is believed that tuning of the ring by external hybrid phase shifters will work even better than in some of the previous tests. A great deal of arcing has been experienced in these hybrids during the numerous tests performed in the past quarter simply because of initial mismatches in test components. Thermally induced mismatches, as circulating power is increased to very high levels, have also been a problem.

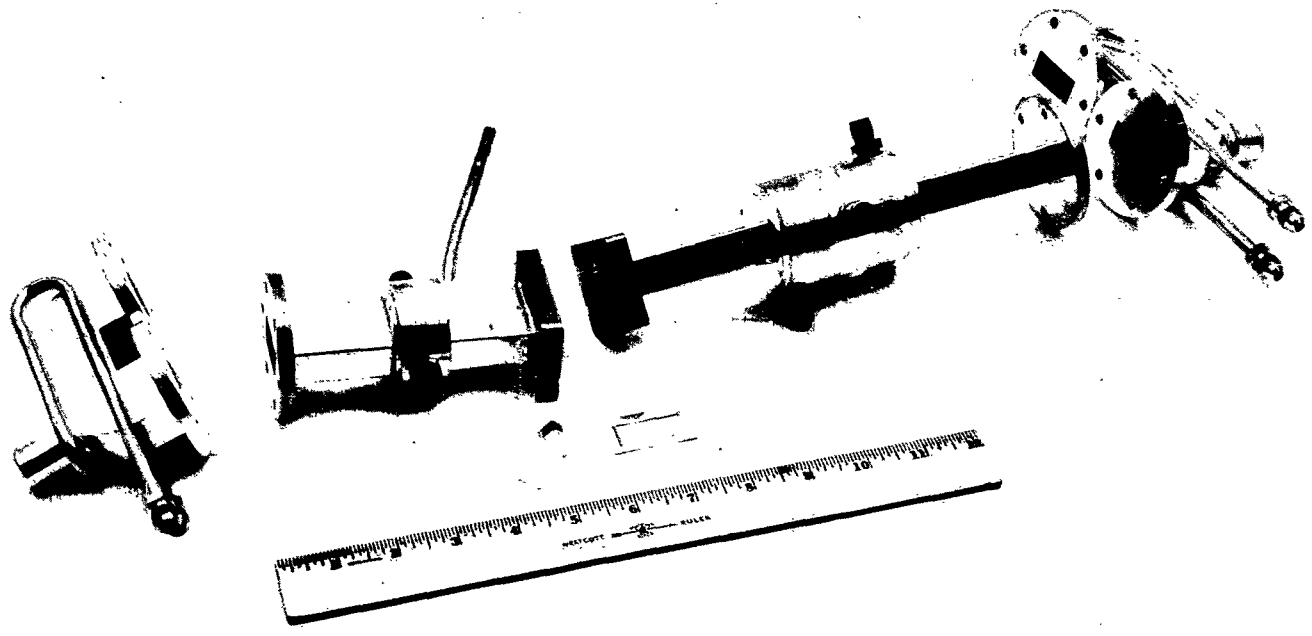

FIGURE 19
COMPONENTS OF WINDOWTRON ASSEMBLY

SECTION III

PROGRAM FOR NEXT QUARTER

High power testing of the new, bakeable windowtron assembly will begin early in the fourth quarter. Both parts of the first windowtron will also be tested individually in a nitrogen pressurized atmosphere.

Evaluation of the effects of gaseous dielectric and air cooling will be made with the double disc assembly described in this report. The effectiveness of air cooling can be determined because of the double cooling system built into this window.

The windowtron will be used as a device to measure and evaluate the effects on power handling of small variations in gas pressure in the 10^{-4} to 10^{-8} Torr range depending on the success achieved in controlling these pressures at a predetermined level. Multipactor in the evacuated region will be studied to see how dependent it is on waveguide pressure. The effects of stray magnetic fields, and the effect of electron sources on multipactor will also be examined.

Continued effort will be directed to the fabrication and testing of several more 25 per cent bandwidth, fluid dielectric cooled double disc windows. The metallizing of the required ceramics is nearly complete and fabrication of the assemblies will begin during April. The ceramic materials now in process for use in these assemblies are AL300 and AL400. Two 1 1/4-inch diameter sapphire discs are also on hand for use in this type of assembly, but no cold tests have been made as yet.

Depending on the results of high power windowtron tests, the program for the fourth quarter may be altered in some details. For example, the use of secondary emission reducing coatings has not been necessary on alumina ceramic block windows because of their obvious failure from poor thermal properties. Beryllia blocks have not failed due to this cause, but may fail because of multipactor discharges. This also applies to the thin disc windows. If this type of failure is experienced, a new look at coatings will be made.

SECTION IV

REFERENCES

1. E. L. Ginzton, Microwave Measurements, (New York: McGraw-Hill, 1957), pp. 321, 335.

2. S. Ramo and J. R. Whinnery, Fields And Waves In Modern Radio, (2nd ed.; Wiley, 1953), p. 461.

3. Quarterly Technical Note No. 2, High Power R-F Window Study Program, RADC-TDR-63-32, furnished by Varian Associates under Contract No. AF 30(602)-2844.

4. A. Staprans and S. Mercer, unpublished Varian Associates Memorandum.

5. Second Quarterly Progress Report, Investigation of Microwave Window Failure Mechanisms and Their Elimination, Sperry Gyroscope Company for USAERDL under Contract NR 36-039SC-87389.

6. R. C. Johnson, "Design of Linear Double Tapers In Rectangular Waveguides," PGMTT, July 1959, p. 374.

7. N. Marcuvitz, Waveguide Handbook, Radiation Laboratories Series, (New York: McGraw Hill, 1951, Vol. 10), Chapter 3.

8. R. E. Collins and J. Brown, "The Calculation of the Equivalent Circuit of an Axially Unsymmetrical Waveguide Junction," Proceedings of the Institution of Electrical Engineers, Vol. 103, Part C, 1956, p. 121.

9. L. B. Felsen and A. A. Oliner, "Determination of Equivalent Circuit Parameters for Dissipative Microwave Structures," Proceedings of the Institute of Radio Engineers, Vol. 42, No. 2, 1954, p. 477.

10. F. L. Wentworth and D. R. Barthel, "A Simplified Calibration of Two Port Transmission Line Devices," Trans. of Institute of Radio Engineers, Vol. MTT-4, No. 3, July 1956, p. 173.

11. J. E. Storer, L. S. Sheingold and S. Stein, "A Simple Graphical Analysis of a Two Part Waveguide Junction," Proceedings of the Institute of Radio Engineers, Vol. 41, No. 8, August 1953, p. 1004.

12. G. A. Deschamps, "Determination of Reflection Coefficients and Insertion Loss of a Waveguide Junction," Journal of Applied Physics, Vol. 24, No. 8, August 1953.

APPENDIX

DERIVATION OF A COMPLEX SCATTERING MATRICE EQUATION FOR WINDOW SYNTHESIS

In Section II of this report a general solution for optimizing the reflection coefficient of a window across a band of frequencies was first considered and then applied to the more specific Symons-type thin disc window. A model for a double disc window showing the component matrices appears in Figure A-1. The derivation of the scattering coefficients and transmission parameters will be pursued here for this window. An identical approach can be used for any thickness of window, or windows in either rectangular or circular configurations using any number of matching components.

A. DETERMINATION OF MATRICES $[T^a]$ and $[T^k]$

The scattering equations

$$b_1 = s_{11}\, a_1 + s_{12}\, a_2$$
$$b_2 = s_{12}\, a_1 + s_{22}\, a_2 \qquad (1a)$$

where a and b are the incident and reflected complex wave amplitudes, respectively, and S_{nm} are the scattering coefficients as defined by Ginzton[1] and can be rearranged as shown in Equation (2a). By solving equations (1a) for b_2 and a_2

$$b_2 = \left(s_{12} - \frac{s_{11}\, s_{22}}{s_{12}}\right) a_1 + \frac{s_{22}}{s_{12}}\, b_1$$
$$a_2 = -\frac{s_{11}}{s_{12}}\, a_1 + \frac{1}{s_{12}}\, b_1 \qquad (2a)$$

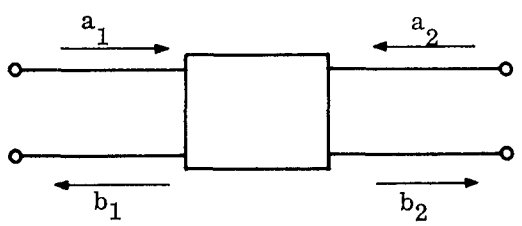

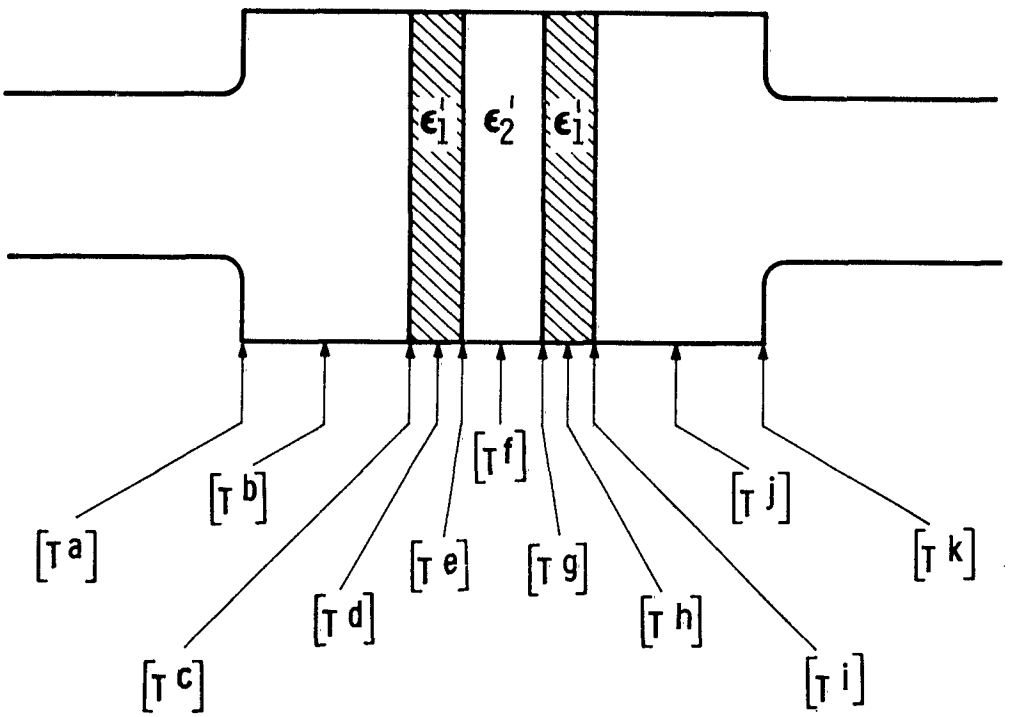

FIGURE A-1
DOUBLE DISC WINDOW MODEL
SHOWING MATRIX DESIGNATIONS

The coefficients are now by definition[2] equal to the transmission parameters or

$$T_{11}^{a} = s_{12} - \frac{s_{11}\, s_{22}}{s_{12}}$$

$$T_{12}^{a} = \frac{s_{22}}{s_{12}} \qquad (3a)$$

$$T_{21}^{a} = -\frac{s_{11}}{s_{12}}$$

$$T_{22}^{a} = \frac{1}{s_{12}}$$

Similarly, by looking into the right hand end of the network and getting a_1 and b_1 in terms of a_2 and b_2

$$b_1 = \left(s_{12} - \frac{s_{11}\, s_2}{s_{12}}\right) a_2 + \frac{s_{11}}{s_{12}}\, b_2 \qquad (4a)$$

$$a_1 = -\frac{s_{22}}{s_{12}}\, a_2 + \frac{1}{s_{12}}\, b_2$$

The corresponding transmission parameters for the $\left[T^{k}\right]$ matrix are

$$T_{11}^{k} = s_{12} - \frac{s_{11}\, s_{22}}{s_{12}}$$

$$T_{12}^{k} = \frac{s_{11}}{s_{12}} \qquad (5a)$$

$$T_{21}^{k} = -\frac{s_{22}}{s_{12}}$$

$$T_{22}^{k} = \frac{1}{s_{12}}$$

Thus, it has been shown that

$$T_{11}^{a} = T_{11}^{k}$$

$$T_{12}^{a} = -T_{21}^{k}$$

$$T_{21}^{a} = -T_{12}^{k} \qquad (6a)$$

$$T_{22}^{a} = T_{22}^{k}$$

Therefore the transmission parameters for the abrupt transitions on either end of the window have been defined in terms of the scattering matrices.

Using the traveling wave equations

$$V = a + b \qquad (7a)$$

and

$$I = \frac{1}{Z_o}(a - b)$$

or

$$\frac{V}{I} = Z = Z_o \frac{(a + b)}{(a - b)} \qquad (8a)$$

$$\frac{Z}{Z_o} = \frac{1 + \frac{b}{a}}{1 - \frac{b}{a}}$$

as

$$\rho = \frac{b}{a} \quad \text{then} \quad \frac{Z}{Z_o} = \frac{1 + \rho}{1 - \rho} \equiv z \qquad (9a)$$

also

$$\rho = \frac{z - 1}{z + 1} \qquad (10a)$$

The scattering coefficients have been defined[1] in terms of the reflection coefficient, ρ.

$$s_{11} = \rho_o \tag{11a}$$

$$s_{22} = \frac{2\rho_o - \rho_{sc} - \rho_{oc}}{\rho_{sc} - \rho_{oc}} \tag{12a}$$

$$\Delta s = s_{11}\, s_{22} - s_{12}^2 = \frac{\rho_o \left(\rho_{oc} + \rho_{sc}\right) - 2\,\rho_{sc}\,\rho_{oc}}{\rho_{sc} - \rho_{oc}} \tag{13a}$$

where

ρ_o = matched load terminated reflection coefficient

ρ_{sc} = short circuited reflection coefficient

ρ_{oc} = open circuited reflection coefficient

These reflection coefficients can be derived by using impedances z_1, a_2 and z_3 as measured by techniques outlined in references 1, 2, and 7 through 12.

$$\rho_o = \frac{z_1 - 1}{z_1 + 1}$$

$$\rho_{sc} = \frac{z_2 - 1}{z_2 + 1} \tag{14a}$$

$$\rho_{oc} = \frac{z_3 - 1}{z_3 + 1}$$

If the short circuit plane, which is chosen so that it does not shift with frequency, is taken as the reference plane, then $z_3 = 0$ or $\rho_{sc} = -1$. Using this condition

$$s_{11} = \frac{z_1 - 1}{z_1 + 1}$$

$$s_{22} = \frac{z_3 \left(z_1 - 1\right) + 2z_1}{z_3 \left(z_1 + 1\right)} \tag{15a}$$

$$s_{12}^2 - s_{11}\, s_{22} = \frac{z_3\left(z_1+1\right) - 2z_1}{z_3\left(z_1+1\right)} \tag{15a}$$

Substituting Equation (15a) into Equation (5a) gives

$$\left[T^a\right] = \frac{1}{s_{12}} \begin{bmatrix} \dfrac{z_3\left(z_1+1\right) - 2z_1}{z_3\left(z_1+1\right)} & -\dfrac{z_3\left(z_1-1\right) - 2z_1}{z_3\left(z_1+1\right)} \\ -\dfrac{z_1-1}{z_1+1} & 1 \end{bmatrix} \tag{16a}$$

and

$$\left[T^k\right] = \frac{1}{s_{12}} \begin{bmatrix} \dfrac{z_3\left(z_1+1\right) - 2z_1}{z_3\left(z_1+1\right)} & \dfrac{z_1-1}{z_1+1} \\ \dfrac{z_3\left(z_1-1\right) + 2z_1}{z_3\left(z_1+1\right)} & 1 \end{bmatrix} \tag{17a}$$

Thus $\left[T^a\right]$ and $\left[t^k\right]$ are determined.

B. DETERMINATION OF MATRICES FOR SECTIONS OF UNIFORM TRANSMISSION LINES

The transmission matrix parameters for uniform transmission line are of the form

$$\begin{bmatrix} e - j\beta L & o \\ o & ej\beta L \end{bmatrix}$$

and will be used in matrices $\left[T^b\right]$, $\left[T^d\right]$, $\left[T^f\right]$, $\left[T^b\right]$, and $\left[T^j\right]$.

$$\beta = \omega\sqrt{\mu\epsilon}\left[1 - \left(f^c/f\right)^2\right]^{1/2} \tag{18a}$$

$\epsilon = \epsilon_o \epsilon^1$

ϵ_o = dielectric constant of free space

ϵ^1 = relative dielectric constant

For the TE_{11}^o mode under consideration

$$fc = \frac{.29306}{r\sqrt{\mu\epsilon}} = \frac{.29306}{r\sqrt{\mu\epsilon_o}\sqrt{\epsilon^1}} \tag{19a}$$

and the expression for β reduces to

$$\beta = \frac{2\pi}{\lambda o}\left[\epsilon^1 - \left(\frac{.29306\lambda o}{r}\right)^2\right]^{1/2}$$

where r = radius of the cylindrical waveguide, and

$$\lambda o = \frac{c}{f}, \quad c = 2.99776 \times 10^{10} \text{ cm/sec}$$

The magnitude of β can now be calculated for each matrix when the relative dielectric constant of the material in that particular section of transmission line is known. The lengths L_b, Ld, Lf, Lb and Lj can either be preselected or can serve as a variable in the computer program.

C. DETERMINATION OF DIELECTRIC INTERFACE MATRICES

The tangential components of electric and magnetic field across a dielectric boundary are continuous or

$$E_{t1} = E_{t2} \text{ and } H_{t1} = H_{t2}$$

In terms of the incident and reflected wave amplitudes are

$$a_1 + b_1 = a_2 + b_2 \tag{20a}$$

and

$$\frac{1}{Z_{01}}\left(a_1 - b_1\right) = -\frac{1}{Z_{02}}\left(a_2 - b_2\right) \tag{21a}$$

Because of the conversion of sign conventions from

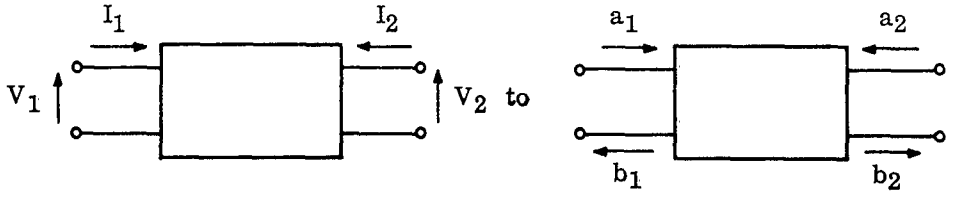

In other words

$$V_1 = V_2$$
$$I_1 = -I_2 \tag{22a}$$

Defining $R = \frac{Zo2}{Zo1}$ and rearranging Equations (20a) and (22a)

$$b_2 = a_1\left(\frac{1+R}{2}\right) + b_1\left(\frac{1-R}{2}\right)$$
$$a_2 = a_1\left(\frac{1-R}{2}\right) + b_1\left(\frac{1+R}{2}\right) \tag{23a}$$

The transmission parameters for these two equations are

$$T_{11} = T_{22} = \frac{1+R}{2}$$
$$T_{12} = T_{21} = \frac{1-R}{2} \tag{24a}$$

For an interface from an air-filled cylindrical guide to a dielectric-filled cylindrical guide carrying the $TE_{11}{}^{o}$ mode where

$$\lambda g = \lambda o \left[\epsilon_1^1 - \left(\frac{.29306\lambda o}{r}\right)^2\right]^{-1/2}$$

then

$$R_1 = \frac{Zo\ air}{Zo\ diel} = \frac{\lambda g\ air}{\lambda g\ diel}$$

$$R_1 = \left[\frac{\epsilon_1^1 - \left(\frac{.29306\lambda o}{r}\right)^2}{1 - \left(\frac{.29306\lambda o}{r}\right)^2}\right]^{1/2} \tag{25a}$$

This result can be substituted into the matrix to get $\left[T^c\right]$

$$\left[T^c\right] = \begin{bmatrix} \frac{1+R_1}{2} & \frac{1-R_1}{2} \\ \frac{1-R_1}{2} & \frac{1+R_1}{2} \end{bmatrix} \tag{26a}$$

Similar derivations must be made for each interface such as shown at T^e, T^j and T^i where the variables are free space wavelength, guide radius and dielectric constant when using the TE_{11}^o transmission mode.

The final complex matrix product for the window of Figure A-1 is

$$\left[T\right] = \left[T^a\right] \left[T^b\right] \left[T^c\right] \ldots \left[T^i\right] \left[T^j\right] \left[T^i\right] \tag{27a}$$

DISTRIBUTION LIST

Copy No.	No. of Copies	Address
1	1	**RADC (RALTP, ATTN: D. Bussey) Griffiss AFB NY
2	1	*RADC (RAAPT) Griffiss AFB NY
3	1	*RADC (RAALD) Griffiss AFB NY
4	1	*GEEIA (ROZMCAT) Griffiss AFB NY
5	1	*RADC (RAIS, ATTN: Mr. Malloy) Griffiss AFB NY
6	1	US Army Electronics R and D Labs Liaison Officer RADC, Griffiss AFB NY
7	1	*AUL (3T) Maxwell AFB Ala
8	1	ASD (ASAPRD) Wright-Patterson AFB Ohio
9	1	Chief, Naval Research Lab ATTN: Code 2027 Wash 25 DC
10	1	Air Force Field Representative Naval Research Lab ATTN: Code 1010 Wash 25 DC
11	1	Commanding Officer US Army Electronics R and D Labs ATTN: SELRA/SL-ADT Ft Monmouth NJ
12	1	National Aeronautics and Space Admin Langley Research Center Langley Station Hampton Virginia ATTN: Librarian
13	1	Central Intelligence Agency ATTN: OCR Mail Room 2430 E Street NW Wash 25 DC
14	1	US Strike Command ATTN: STRJ5-OR Mac Dill AFB Fla
15	1	AFSC (SCSE) Andrews AFB Wash 25 DC
16	1	Commanding General US Army Electronic Proving Ground ATTN: Technical Documents Library Ft Huachuca Ariz
17 - 26	10	*ASTIA (TISIA-2) Arlington Hall Station Arlington 12 Va
27	1	AFSC (SCFRE) Andrews AFB Wash 25 DC
28	1	Hq USAF (AFCOA) Wash 25 DC
29	1	AFOSR (SRAS/Dr. G. R. Eber) Holloman AFB NMex
30	1	Office of Chief of Naval Operations (Op-724) Navy Dept Wash 25 DC
31	1	Commander US Naval Air Dev Cen (NADC Lib) Johnsville Pa
32	1	Commander Naval Missile Center Tech Library (Code NO 3022) Pt Mugu Calif
33	1	Bureau of Naval Weapons Main Navy Bldg Wash 25 DC ATTN: Technical Librarian, DLl-3
34	1	Redstone Scientific Information Center US Army Missile Command Redstone Arsenal, Alabama
35	1	Commandant Armed Forces Staff College (Library) Norfolk 11 VA
36	1	ADC (ADOAC-DL) Ent AFB Colo
37	1	AFFTC (FTOOT) Edwards AFB Calif
38	1	Commander US Naval Ordnance Lab (Tech Lib) White Oak, Silver Springs Md
39	1	Commanding General White Sands Missile Range New Mexico ATTN: Technical Library
40	1	Director US Army Engineer R and D Labs Technical Documents Center Ft Belvoir VA
41	1	ESD (ESRL) L G Hanscom Fld Bedford Mass
42	1	Commanding Officer and Director US Navy Electronics Lab (LIB) San Diego 52 Calif
43	1	ESD (ESAT) L G Hanscom Fld Bedford Mass
44	1	Commandant US Army War College (Library) Carlisle Barracks Pa
45	1	APGC (PGAPI) Eglin AFB Fla
46	1	AFSWC (SWOI) Kirtland AFB NMex
47	1	Dr. A. Pronner Litton Industries 960 Industrial Road San Carlos Calif
48	1	Mr. Del Churchill Sperry Gyroscope Co Great Neck NY
49	1	ARPA ATTN: Col Lindsay Washington 25 DC
50	1	RTD (RTGS) Bolling AFB Washington 25 DC
51	1	Dr. Louis R. Bloom Sylvania Elect Prod Inc Physics Lab 208-20 Willetts Point Blvd Bayside, Long Island NY

*Mandatory

**Project Engineer will enter his symbol and

DISTRIBUTION LIST

Copy No.	No. of Copies	Address
1	1	**RADC (RALTP, ATTN: D. Bussey) Griffiss AFB NY
2	1	*RADC (RAAPT) Griffiss AFB NY
3	1	*RADC (RAALD) Griffiss AFB NY
4	1	*GEEIA (ROZMCAT) Griffiss AFB NY
5	1	*RADC (RAIS, ATTN: Mr. Malloy) Griffiss AFB NY
6	1	US Army Electronics R and D Labs Liaison Officer RADC, Griffiss AFB NY
7	1	*AUL (3T) Maxwell AFB Ala
8	1	ASD (ASAPRD) Wright-Patterson AFB Ohio
9	1	Chief, Naval Research Lab ATTN: Code 2027 Wash 25 DC
10	1	Air Force Field Representative Naval Research Lab ATTN: Code 1010 Wash 25 DC
11	1	Commanding Officer US Army Electronics R and D Labs ATTN: SELRA/SL-ADT Ft Monmouth NJ
12	1	National Aeronautics and Space Admin Langley Research Center Langley Station Hampton Virginia ATTN: Librarian
13	1	Central Intelligence Agency ATTN: OCR Mail Room 2430 E Street NW Wash 25 DC
14	1	US Strike Command ATTN: STRJ5-OR Mac Dill AFB Fla
15	1	AFSC (SCSE) Andrews AFB Wash 25 DC
16	1	Commanding General US Army Electronic Proving Ground ATTN: Technical Documents Library Ft Huachuca Ariz
17 - 26	10	*ASTIA (TISIA-2) Arlington Hall Station Arlington 12 Va
27	1	AFSC (SCFRE) Andrews AFB Wash 25 DC
28	1	Hq USAF (AFCOA) Wash 25 DC
29	1	AFOSR (SRAS/Dr. G. R. Eber) Holloman AFB NMex
30	1	Office of Chief of Naval Operations (Op-724) Navy Dept Wash 25 DC
31	1	Commander US Naval Air Dev Cen (NADC Lib) Johnsville Pa
32	1	Commander Naval Missile Center Tech Library (Code NO 3022) Pt Mugu Calif
33	1	Bureau of Naval Weapons Main Navy Bldg Wash 25 DC ATTN: Technical Librarian, DLl-3
34	1	Redstone Scientific Information Center US Army Missile Command Redstone Arsenal, Alabama
35	1	Commandant Armed Forces Staff College (Library) Norfolk 11 VA
36	1	ADC (ADOAC-DL) Ent AFB Colo
37	1	AFFTC (FTOOT) Edwards AFB Calif
38	1	Commander US Naval Ordnance Lab (Tech Lib) White Oak, Silver Springs Md
39	1	Commanding General White Sands Missile Range New Mexico ATTN: Technical Library
40	1	Director US Army Engineer R and D Labs Technical Documents Center Ft Belvoir VA
41	1	ESD (ESRL) L G Hanscom Fld Bedford Mass
42	1	Commanding Officer and Director US Navy Electronics Lab (LIB) San Diego 52 Calif
43	1	ESD (ESAT) L G Hanscom Fld Bedford Mass
44	1	Commandant US Army War College (Library) Carlisle Barracks Pa
45	1	APGC (PGAPI) Eglin AFB Fla
46	1	AFSWC (SWOI) Kirtland AFB NMex
47	1	Dr. A. Pronner Litton Industries 960 Industrial Road San Carlos Calif
48	1	Mr. Del Churchill Sperry Gyroscope Co Great Neck NY
49	1	ARPA ATTN: Col Lindsay Washington 25 DC
50	1	RTD (RTGS) Bolling AFB Washington 25 DC
51	1	Dr. Louis R. Bloom Sylvania Elect Prod Inc Physics Lab 208-20 Willetts Point Blvd Bayside, Long Island NY

*Mandatory

**Project Engineer will enter his symbol and

DISTRIBTUION LIST (Cont.)

Copy No.	No. of Copies	Address
52 - 53	2	Technical Library Varian Associates 611 Hansen Way Palo Alto, California
54	1	Dr. L. A. Roberts Watkins Johnson Co Palo Alto, California
55	1	Mr. Gerald Klein, Mgr Microwave Tube Section Applied Research Dept Westinghouse Elect Corp Friendship Intl Airport Box 746 Baltimore, Md.
56	1	Hughes Aircraft Co Culver City, Calif ATTN: Everett M. Wallace
57	1	Bendix Aviation Corp Red Bank Division Eatontown, New Jersey ATTN: John Johnstone
58 - 59	2	Eitel Mc Cullough Inc 901 Industrial Way San Carlos, California ATTN: Stella R. Vetter Research Library
60	1	Mr. F. E. Ferrira Director of Research Coors Porcelain Co Golden, Colorado
61 - 62	2	Mr. M. Hoover RCA Lancaster, Pa
63	1	Dr. D. Goodman Sylvania Microwave Tube Lab 500 Evelyn Avenue Mt. View, California
64	1	Mr. A. E. Harrison University of Washington Dept of Elect Engineering Seattle 5, Washington
65	1	Mr. Shelden S. King Eng Librarian Westinghouse Elect Corp PO Box 284 Elmira, New York
66	1	Kane Engineering Labs 845 Commercial Street Palo Alto, California ATTN: Mr. F. Kane
67	1	Electrical Industries Co Murray Hill, New Jersey ATTN: Mr. Peter A. Muto
68	1	Mr. L. E. Gates, Jr. 20/1365 41-48-20 Hughes Aircraft Co Culver City, California
69	1	Mr. Theodore Poumbanis Microwave Elect Prod Inc Microwave Device Operations 600 Evelyn Avenue Mountain View, California
70	1	Dr. R. G. E. Hutter Sylvania Microwave Tube Lab 500 Evelyn Ave Mt. View, California
71	1	Dr. William Watson Litton Industries 960 Industrial Road San Carlos, Calif
72	1	Technical Library Litton Industries 960 Industrial Road San Carlos, Calif
73	1	Mr. Ted Moreno Varian Associates 611 Hansen Way Palo Alto, Calif
74	1	Mr. C. Dalman Cornell University Dept of Elect Eng Ithaca, New York
75	1	Mr. Donald Priest Eitel-Mc Cullough Inc San Bruno, California
76	1	Mr. T. Marchese Federal Tele Labs Inc 500 Washington Ave Nutley, New Jersey
77	1	Mr. S. Webber General Elect Microwave Lab 601 California Ave Palo Alto, California
78	1	Mr. Lester Firestein Stanford Research Institute Palo Alto, California
79	1	Dr. D. D. King Johns Hopkins University Radiation Laboratory Baltimore 2, Maryland
80	1	Mr. R. Butman M.I.T. Lincoln Laboratory PO Box 73 Lexington 73, Mass.
81	1	Dr. S. F. Kaisel Microwave Electronics Corp 4061 Transport Street Palo Alto, California
82	1	Ohio State University Dept of Elect Engineering Columbus 10, Ohio ATTN: Prof. E. M. Boone
83	1	Mr. W. C. Brown Spencer Lab Raytheon Mfg Co Wayside Rd Burlington, Mass.
84	1	Mr. W. Teich Raytheon Mfg Co Spencer Lab Burlington, Mass.
85	1	Mr. Hans Jenny RCA Elect Tube Div 415 South 5th Street Harrison, New Jersey
86	1	Mr. P. Bergman Sperry Corp Elect Tube Div Gainesville, Florida
87	1	Dr. M. Chodorow Stanford University Microwave Lab Stanford, California
88	1	Dr. Bernard Arfin Varian Associates 611 Hansen Way Palo Alto, California
89	1	Dept of Electrical Eng University of Florida Gainsville, Florida
90	1	Dr. E. D. Mc Arthur General Elect Co Electron Tube Div of Research Lab The Knolls Schenectady, New York
91	1	Mr. J. T. Milek Hughes Aircraft Co Electron Tube Laboratory Culver City, California
92	1	University of Illinois Electrical Eng Research Lab Urbana, Ill ATTN: Technical Editor

DISTRIBUTION LIST (Cont.)

Copy No.	No. of Copies	Address
93	1	Dr. Norman Moore Litton Industries 960 Industrial Road San Carlos, California
94	1	Mass Institute of Technology Research Laboratory of Electronics Cambridge 39, Mass. ATTN: Document Library
95	1	University of Minnesota Minneapolis, Minnesota ATTN: Dr. W. G. Shepherd Dept of Elect Eng
96	1	Dr. M. Ettinberg, Polytechnic Institute of Brooklyn Microwave Research Inst Brooklyn 1, New York
97	1	Mr. John M. Osepchuk Raytheon Co Spencer Lab Burlington, Mass
98	1	Dr. Bernard Hershenon RCA Labs Princeton, New Jersey
99	1	Dr. W. M. Webster Director Electronic Research Lab RCA Labs Princeton, New Jersey
100	1	Stanford University Elect Research Laboratory Stanford, California ATTN: Mr. D. C. Bacon Asst Director
101	1	Dr. D. A. Watkins Stanford University Electronics Laboratory Stanford, California
102	1	Secretariat Advisory Group on Electron Tubes 346 Broadway New York 13, New York
103	1	Bell Telephone Labs Murry Hill Laboratory Murry Hill, New Jersey ATTN: Dr. J. R. Pierce
104	1	Mr. A. G. Peifer Research Laboratories Div The Bendix Corporation Southfield Detroit, Michigan
105	1	Professor R. M. Saunders University of California Dept of Engineering Berkeley 4, California
106 - 107	2	Commanding Officer US Army Signal R and D Lab ATTN: Logistics Div (SIGRA/SL-PRT) L. N. Heynick Ft. Monmouth New Jersey
108	1	Field Emession Corp. 611 Third Street McMinnville Oregon ATTN: Mr. F. M. Charbonnier
109	1	Dr. Robert T. Young Chief Electron Tube Branch Diamond Ord Fuse Lab Washington 25, D.C.
110	1	Applied Radiarion Co Walnut Creek California ATTN: Mr. Niel J. Norris
111	1	RTD (RTH) Bolling AFB Washington 25, D.C.
112	1	The Electronics Research Lab 427 Cory Hall The University of California Berkeley 4, California ATTN: Mrs. Simmons
113	1	Professor W. G. Worcester University of Colorado Dept of Electrical Engineering Boulder, Colorado
114	1	Columbia University Columbia Radiation Lab 538 W 120th Street New York 27, N.Y.
115	1	NAFEC Library Bldg. 3 Atlantic City, N. J.
116 - 119	4	RADC(RALTP, Attn: D. Bussey) GRIFFISS AFB, N. Y.
120 - 140	21	Retained by Varian Associates